THE ROYAL SOCIETY

Longitudinal dispersion by bodies fixed in a potential flow

BY I. EAMES[1] AND J. W. M. BUSH[2]

[1]*School of Mathematics, Bristol University, University Walk, Bristol BS8 1TW, UK*

[2]*Department of Mathematics, MIT, 77 Massachusetts, 2-382, Cambridge, MA 02139, USA*

Received 10 December 1998; accepted 12 March 1999

We examine tracer dispersion by the potential flow through a random array of rigid bodies fixed relative to a mean flow. Both Darcy flow through permeable bodies and inviscid irrotational flow past impermeable bodies are treated within one theoretical framework. The variation of the longitudinal dispersivity with body shape and permeability κ is examined for the case of high Péclet number, Pe. In the absence of diffusive effects, the longitudinal dispersivity $\mathcal{D}_{xx}$ (where the mean flow is parallel to the x-axis) is calculated by tracing the evolution of a material surface advected by the mean flow and distorted by the array of bodies. For a random array of identical bodies of volume $\mathcal{V}$ and low volume fraction α, $\mathcal{D}_{xx} = \alpha|D_f|UL/\mathcal{V}$. The drift volume, D_f, is defined as the volume between the final and initial position of a material surface distorted by a single body moving in an unbounded flow, and L is the length-scale characterizing the associated longitudinal displacement of the surface. The variation of $\mathcal{D}_{xx}$ with permeability is illustrated by considering permeable cylinders and spheres, and the effect of body shape on dispersion is illustrated by considering impermeable spheroids.

The longitudinal dispersivity arising from the flow past impermeable bodies is $\mathcal{D}_{xx} = \alpha C_{xx} UL$, where C_{xx} is the added-mass coefficient characterizing the mean flow around the body. This indicates that bluff bodies enhance longitudinal dispersion by promoting the longitudinal stretching of fluid elements. For Darcy flow through bodies of low permeability, the longitudinal dispersivity is $\mathcal{D}_{xx} = \alpha(C_{xx} + 1)UL$. The length-scale L, and thus $\mathcal{D}_{xx}$, is singular as $\kappa \to 0$, owing to the long retention time of fluid within the bodies. For highly permeable two-dimensional bodies, $\mathcal{D}_{xx} = \alpha(C_{yy}+1)UL$, where C_{yy} is the added-mass coefficient characterizing the flow around an impermeable body moving parallel to the y-axis. Consequently, dispersion by highly permeable bodies is enhanced when the bodies are slender, in contrast to the low-permeability limit.

The influence of finite tracer diffusivity on longitudinal dispersion is demonstrated to make a negligible contribution when $\kappa > 0$ provided $Pe \gg \max(1, 1/\kappa)$ and for impermeable bodies provided $Pe \gg 1$. When $Pe \ll 1/\kappa$, the longitudinal dispersion is dominated by diffusive effects and $\mathcal{D}_{xx} = O(\alpha U^2 a^2/\mathcal{D}_1)$.

Keywords: porous media; dispersion; drifts

1. Introduction

In a variety of physical situations, the dispersion of a tracer material suspended in a fluid is dominated by the impact of discrete bodies on a mean flow. Tracer transport is influenced by both convective and diffusive processes, whose relative importance is characterized by the Péclet number, $Pe = Ua/\mathcal{D}$, defined in terms of a characteristic body length-scale a, mean fluid speed U and tracer diffusivity $\mathcal{D}$. In this paper we examine dispersion by the potential flow through an array of bodies for the two regimes of high and low Pe, and pay particular attention to the influence of body shape and permeability on longitudinal dispersivity.

The influence of inhomogeneities on the flow through a saturated porous media is important in both oil recovery and the modelling of groundwater flows (Dagan 1987). Modelling dispersion in porous media generally requires consideration of the flow on both micro- and macroscopic scales. The microscale flow is typically described by Stokes flow, while the macroscale flow is described by Darcy's law, and so corresponds to a potential flow. Microscale dispersion in a porous media is influenced by the topology of the porous matrix, in particular by the tortuosity of the paths taken by fluid elements passing through the matrix. Koch & Brady (1985) examined microscale dispersion in porous media by modelling the porous matrix as a dilute random array of spherical bodies. At high Péclet number, Koch & Brady (1985) demonstrated that there are a number of different processes contributing to the longitudinal dispersivity: a mechanical component, $\frac{3}{4}aU$, associated with the passive advection of material (and independent of volume fraction); a non-mechanical component, $\frac{1}{6}\pi^2\alpha aU\log(Pe)$, associated with the no-slip condition on the surface of the spheres (Saffman 1959); and a contribution from the tracer hold-up within the spherical particles. The longitudinal dispersion arising from the flow through a fixed array of permeable beads was recently studied by Magnico *et al.* (1993), who generated the beads (of typical diameter 600 μm) by sintering glass spheres of diameter 55 or 110 μm. As the permeability of the beads was reduced, the longitudinal dispersivity increased dramatically, owing to the long-time retention of fluid within the beads.

Macroscale dispersion in porous media arises from large-scale variations in permeability, and in certain instances dominates the contribution from microscale diffusion (Dagan 1987). A large number of theoretical studies have examined the influence of spatial variations in permeability on dispersion, using as a starting point the assumption that the permeability κ at each position is characterized by a lognormal probability distribution (Freeze 1975). For the specific case that the spatial correlation of $Y = \log\kappa$ decays exponentially over a distance I, Dagan (1984) showed that in both two and three dimensions, the longitudinal dispersivity is $\sigma_Y^2 UI$, where σ_Y^2 is the variance of Y. In this paper we examine the dispersion associated with flow past discrete permeable inclusions which has a bearing on both macroscale dispersion in porous media and, as indicated by the experiments of Magnico *et al.* (1993), on microscale dispersion.

The dispersion associated with high-Reynolds-number flow past bluff bodies is important in a variety of physical systems; for example, in bubble-induced mixing, and in the dispersal of pollutants around groups of buildings (Jerram *et al.* 1995). In high-Reynolds-number flow past a body, the upstream flow may be described to leading order as inviscid; however, viscous effects become important in the neighbourhood of the body, generating vorticity which is advected into the wake of the

body, where the potential flow description breaks down. Nevertheless, potential flow models have been used successfully in the theoretical modelling of high-Reynolds-number flow past bluff bodies. The description of weakly turbulent flow in terms of a potential flow advecting and distorting turbulent eddies has been used to model both the modification of turbulent fields by bluff bodies (Hunt 1973) and dispersion past two-dimensional bluff bodies (Hunt & Mulhearn 1973). Drazin (1961) demonstrated that strongly stratified flow past obstacles may be described in any horizontal plane as potential flow to leading order, and this description has been adopted by Weng & Carruthers (1994) in characterizing dispersion by wind blowing past hills.

In this paper we calculate the longitudinal dispersivity caused by the potential flow past a random array of bodies which are fixed relative to a mean flow. The effect of body shape and permeability on high Pe dispersion has not to our knowledge been studied previously and characterizing this dependence will be the principal contribution of this paper. The methodology adopted to tackle this problem is based on Darwin's (1953) concept of drift which is ideally suited to studying fluid transport by potential flows. The approach of Koch & Brady (1985) could be applied to this problem; however, the interpretation of the longitudinal dispersivity as a function of body shape does not follow so naturally from their formulation.

We restrict our attention to the study of the dispersive properties of a dilute array of bodies. Since the influence of bodies fixed in potential flows is relatively short-range (with the velocity disturbance decaying as $1/r^3$ from the body), a leading-order description of the flow may therefore be obtained by neglecting the interactions between neighbouring bodies and simply superimposing the effects of individual bodies. In contrast, the description of Stokes flow through an array of bodies is complicated by the long-range influence of the individual bodies on the flow (with the velocity disturbance decaying as $1/r$ from the body). The calculations for the effective dispersivity arising from bodies fixed in a Stokes flow require consideration of the interactions between neighbouring bodies, even when the array is dilute, and are accordingly complex (Koch & Brady 1985).

The paper is structured as follows. In § 2 we present our theoretical model of potential flow through a random array of bodies, which incorporates both perfect flow past impermeable bodies and Darcy flow past porous bodies. In § 3 we consider the distortion of a material surface by potential flow past individual bodies, and characterize the dependence of the form of the distortion on both body shape and permeability. These results are applied in § 4 in describing mechanical dispersion by potential flow through an array of obstacles. The resulting derivation for the coefficient of longitudinal dispersivity is used to develop a simple model of mixing across a horizontal interface in § 5. Diffusive effects at high Pe are analysed in § 6. The relevance of our model of mechanical dispersion to a number of physical systems is discussed in § 7.

2. Problem definition

We consider dispersion by potential flows, which are described in terms of the gradient of a scalar potential ϕ:

$$\boldsymbol{u} = \nabla\phi, \tag{2.1}$$

where $\phi = \phi_1$ inside the body and $\phi = \phi_2$ outside the body, and ϕ satisfies Laplace's equation because the fluid is incompressible. When the bodies are impermeable to

initially located at (x_0, y, z) is advected to

$$x_f(x_0, y, z, t) = x_0 - Ut - \left[\frac{\phi + Ux}{U}\right]_0^t + \int_0^t \frac{|\nabla\phi - \boldsymbol{U}|^2}{U}\,\mathrm{d}t, \tag{3.2}$$

in time t, where the time integral is taken along a streamline. The fluid is advected with speed U, while undergoing a permanent displacement in the fluid frame of reference. The integral term represents a positive 'drift'† component in unbounded flow, the component confined near the point of crossing, while the term in square brackets represents the negative 'reflux' component required by continuity.

Equation (3.2) may be generalized in order to deduce the form of the fluid displacement associated with Darcy flow past a single body of permeability κ embedded in a matrix of unit permeability. We consider a body in a periodic domain $\mathcal{A}$ of cross-sectional area A in order to be able to meaningfully characterize the reflux amplitude, which must vanish in an unbounded domain. By taking into account boundary conditions (2.2*b*) on the body surface, we demonstrate that the fluid displacement is

$$x_f(x_0, y, z, t) = x_0 - Ut - \underbrace{\left[\frac{\phi_2 + Ux}{U}\right]_0^t}_{x_\mathrm{r},\ \text{reflux}} - \underbrace{\frac{(1-\kappa)}{\kappa}\left[\frac{\phi_1}{U}\right]_{t_1}^{t_2} + \int_0^t \frac{|\nabla\phi - \boldsymbol{U}|^2}{U}\,\mathrm{d}t}_{x_\mathrm{d},\ \text{drift}}, \tag{3.3}$$

where the limits t_1 and t_2 refer to interior points on streamlines passing through the body. The expression (3.3) for the fluid displacement is exact and may be adapted to describe the displacement due to the flow through an array of bodies. When $\kappa = 0$, the exterior flow is identical to the flow past an impermeable body so the fluid displacement assumes the form (3.2). When the body is permeable, an additional contribution to drift is made which is either negative or positive depending on whether the body is more ($\kappa > 1$) or less ($\kappa < 1$) permeable than the surrounding material.

For our purposes, it will prove useful to characterize the deformation of a material surface in terms of the total volume of fluid transported forward by the body relative to the flow:

$$D_f = \int_{\mathcal{A}} \lim_{t\to\infty} x_\mathrm{d}(x_0, y, z, t)\,\mathrm{d}A, \tag{3.4}$$

which we henceforth refer to as the 'drift volume', and a length-scale L corresponding to the distance of the centre of volume displaced from the yz-plane:

$$|D_f|L = \frac{1}{2}\int_{\mathcal{A}} (\lim_{t\to\infty} x_\mathrm{d}(x_0, y, z, t))^2\,\mathrm{d}A. \tag{3.5}$$

When the body is moving in irrotational inviscid flow ($\kappa = 0$), D_f corresponds to Darwin's drift volume, and is simply related to the body volume $\mathcal{V}$ through the added-mass coefficient, $\mathcal{D}_{xx} = C_{xx}\mathcal{V}$.

The reflux associated with an isolated body fixed in a periodic domain may be determined by the velocity potential in the far field. In an unbounded flow, the

† In unbounded flow, the drift component is evaluated by subtracting 'reflux' from $x_f(y, z, t)$. When the body is impermeable, the drift term may also be evaluated directly from the integral expression in (3.2).

far-field velocity potential may be described in terms of a dipole of strength d. In a periodic flow, an infinite distribution of such dipoles is required in order to satisfy the kinematic periodicity conditions (see Eames *et al.* 1994, fig. 11). The reflux may be determined by summing the contributions of these dipoles, and we thus demonstrate that the integral of reflux across the periodic flow is

$$\int_{\mathcal{A}} x_{\mathrm{r}}\,\mathrm{d}A = -4\pi d \quad (3\mathrm{D}), \qquad \int_{\mathcal{A}} x_{\mathrm{r}}\,\mathrm{d}A = -2\pi d \quad (2\mathrm{D}). \tag{3.6}$$

The conservation of mass requires that equal volumes of fluid be transported forward and backward:

$$0 = \epsilon\mathcal{V} + \int_{\mathcal{A}} x_{\mathrm{r}}\,\mathrm{d}A + \int_{\mathcal{A}} x_{\mathrm{d}}\,\mathrm{d}A, \tag{3.7}$$

where $\epsilon\mathcal{V}$ is the volume held up by the body. In general, $\epsilon = 0$ for $\kappa > 0$, $\epsilon = 1$ for $\kappa = 0$ and when $\kappa < 0$, ϵ depends on the body shape. The drift volume,† from (3.6) and (3.7), is thus given by

$$D_f = 4\pi d - \epsilon\mathcal{V} \quad (3\mathrm{D}), \qquad D_f = 2\pi d - \epsilon\mathcal{V} \quad (2\mathrm{D}). \tag{3.8}$$

In what follows, we consider in detail the nature of the distortion of the material surface for the two special cases of interest: inviscid flow past impermeable bodies and Darcy flow past permeable bodies.

(*a*) *Impermeable bodies*

When an impermeable body is fixed in an inviscid irrotational flow, $\epsilon = 1$ and the strength of the dipole which characterizes the far-field flow is related to the body volume by (Taylor 1928)

$$d = (C_{xx} + 1)\mathcal{V}/4\pi \quad (3\mathrm{D}), \qquad d = (C_{xx} + 1)\mathcal{V}/2\pi \quad (2\mathrm{D}). \tag{3.9}$$

Equation (3.9) thus indicates that the drift volume is equal to the volume of fluid associated with the added mass of the body: $D_f = C_{xx}\mathcal{V}$, in accordance with Darwin's (1953) proposition.

The dependence of the distortion profile on the bluffness of an impermeable body is illustrated here by considering two-dimensional flow past an elliptical body. The ellipse has half-width a and half-length b, and the flow is described by the velocity potential given by Batchelor (1967, p. 434). The deformation of a material surface by an ellipse inclined to the mean flow is equivalent to the deformation by a cylinder of radius $\frac{1}{2}(a+b)$ (Appendix A). Figure 2*a* shows the effect of varying the aspect ratio of an ellipse aligned with the mean flow on the form of the distorted interface, and demonstrates that the profiles become more peaked as the ellipse becomes more oblate or bluff (figure 2*b*). The drift volume associated with an impermeable ellipse aligned with the mean flow, $D_f = \pi a^2$, is independent of the length of the ellipse. However, the length-scale characterizing the distortion of the material surface, $L/a = 2\mathcal{C}a/(a+b)$ (Appendix A), varies with a/b but tends to a constant $2\mathcal{C}$ as the bluffness of the ellipse increases (figure 2*b*). The constant coefficient $\mathcal{C}$ is defined

† An alternative method of deriving (3.8) may be obtained by modifying Yih's (1985) geometrical derivation of Darwin's proposition.

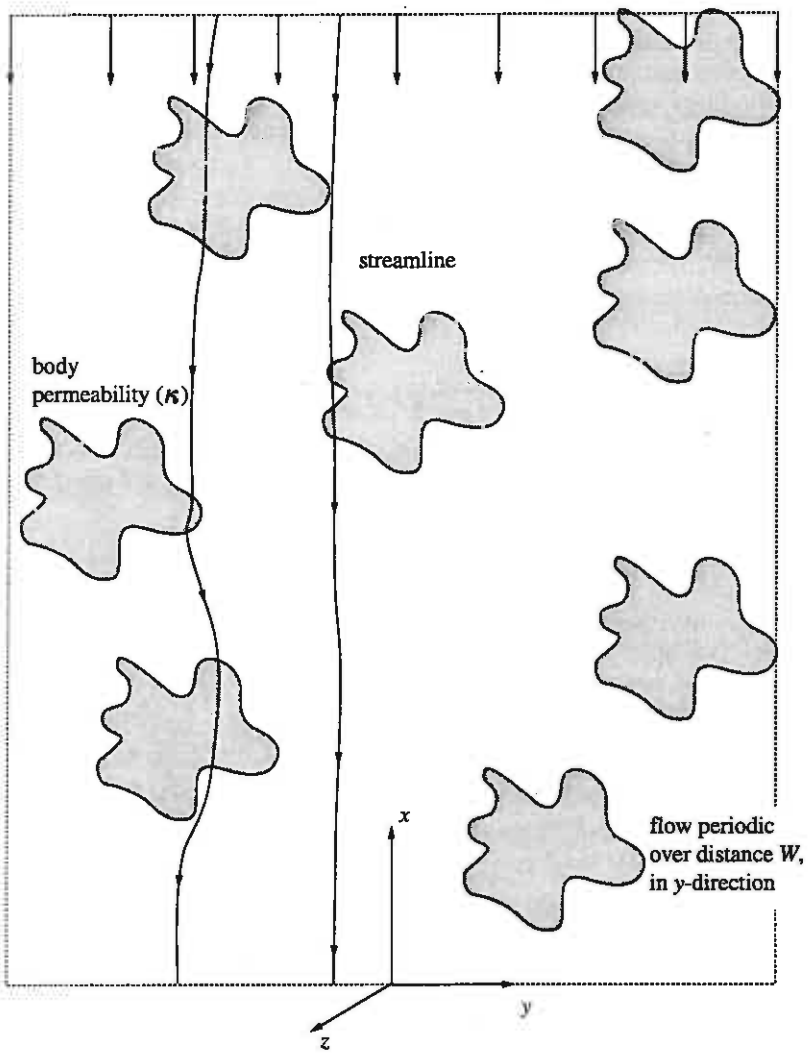

Figure 1. Schematic illustration of the flow through a random array of identical bodies of permeability κ, embedded in a material of unit permeability.

as the value of L/a when $a = b$, and is determined numerically to be $C = 0.74$ from the deformation of a material surface by a cylinder. For comparison, the length-scale L characterizing the distortion of the material surface by the flow past an impermeable ellipsoid aligned with the mean flow (Pozrikidis 1996) is plotted in figure 2*b*. As in the analogous two-dimensional problem, the length-scale L is determined uniquely by the width of the ellipsoid as the aspect ratio increases.

The distortion of a material surface by an oblate ellipse inclined at various angles θ to the mean flow is shown in figure 3*a*. The cross-sectional area presented to the mean flow decreases as θ increases so that the deformation becomes less pronounced. Consequently, the length-scale characterizing the displacement of the material surface,

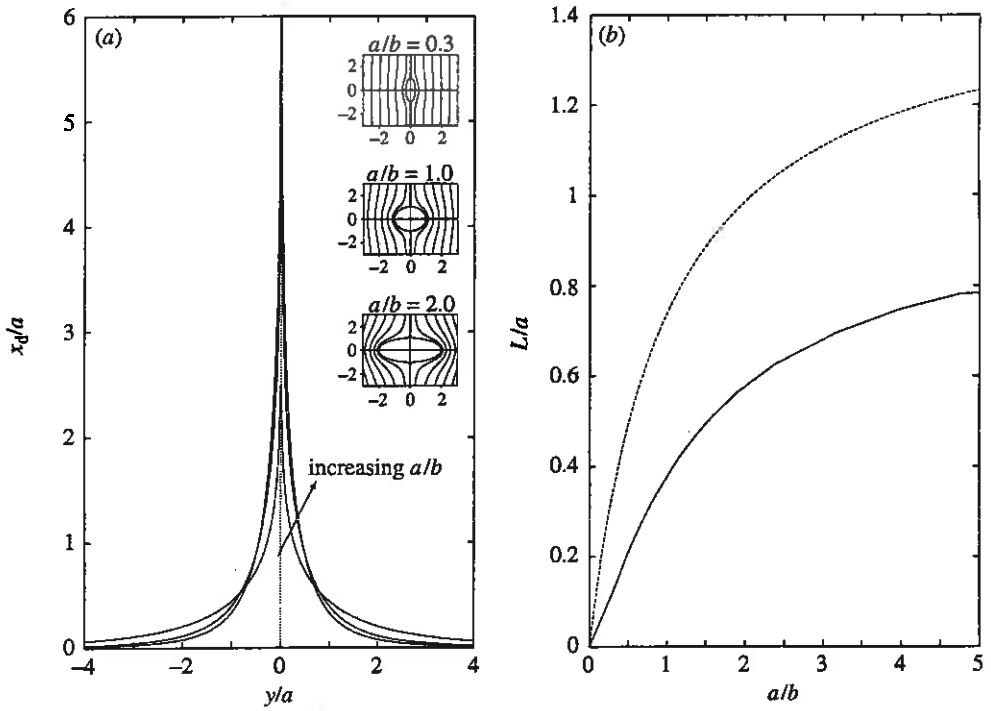

Figure 2. (*a*) The distortion of a material surface by a rigid impermeable ($\kappa = 0$) ellipse for $a/b = 0.3, 1.0, 2.0$. (*b*) The length-scale L characterizing the deformation of the material surface by an ellipse (– – –) and ellipsoid (——).

L, which is given exactly by (Appendix A)

$$\frac{L}{a} = \frac{2\mathcal{C}b}{a+b}\left(\frac{a}{b}\cos^2\theta + \frac{b}{a}\sin^2\theta\right), \tag{3.10}$$

decreases monotonically as θ increases, as indicated in figure 3*b*.

(*b*) *Permeable bodies*

When the body has low permeability, $0 < \kappa \ll 1$, the dipole strength characterizing the far-field flow is identical to that associated with an impermeable body. While no fluid is held up by the body ($\epsilon = 0$), the body itself is saturated with fluid, so that the drift volume, $D_f = (C_{xx} + 1)\mathcal{V}$, is discontinuous at $\kappa = 0$.

When the body is two dimensional and highly permeable ($\kappa \gg 1$), the velocity potential on the body surface satisfies $\phi_2 = 0$ (from (2.2*b*)) and $\phi_2 \to -Ux$ as $|\boldsymbol{x}| \to \infty$. Consequently, in unbounded flow, the isopotential surfaces around a highly permeable body moving parallel to the x-axis correspond precisely to streamlines associated with the flow past an impermeable body (of the same shape) moving parallel to the y-axis, i.e. $\phi_2 = U(x - (C_{yy}+1)\mathcal{V}x/2\pi r^2)$ as $r \to \infty$. Thus, the dipolar strength is $d = -(C_{yy} + 1)\mathcal{V}/2\pi$. From (3.8) the drift volume, $D_f = -(C_{yy} + 1)\mathcal{V}$, is negative in this large-κ limit because fluid permeating through the body travels faster than the mean flow. The difficulty in generalizing this result to arbitrarily shaped

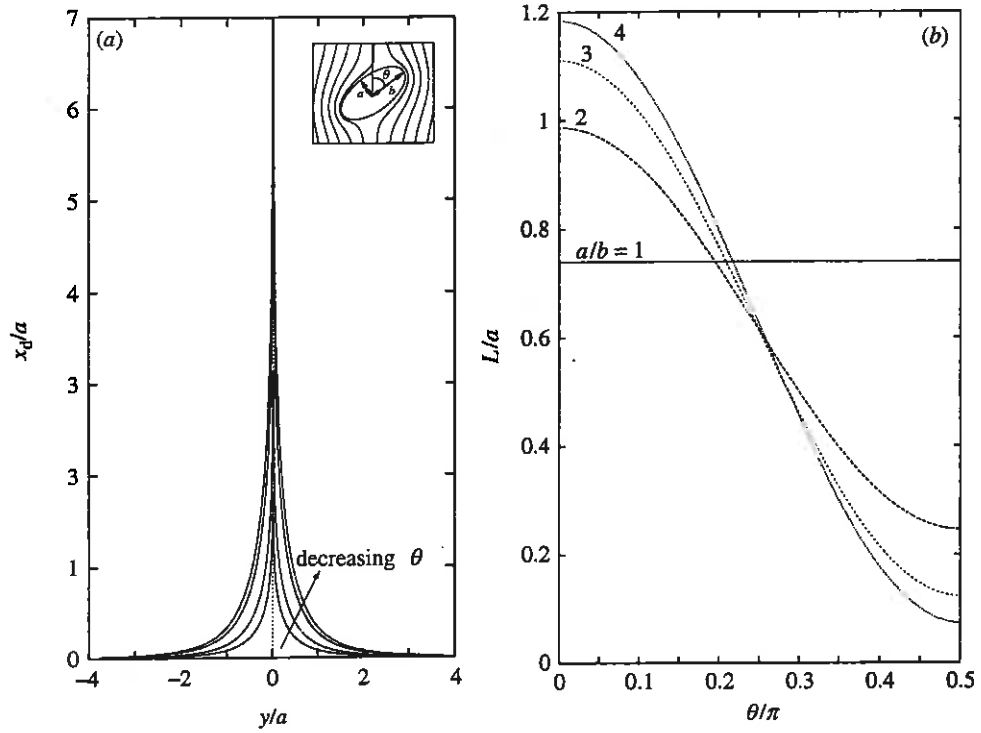

Figure 3. (*a*) The distortion of a material surface by an ellipse inclined to the mean flow at an angle $\theta = 0, \pi/6, \pi/3, \pi/2$. (*b*) The length-scale L characterizing the deformation of the material surface by an ellipse as a function of the orientation to the mean flow, θ.

three-dimensional bodies lies in the fact that the stream-function is not Laplacian in three dimensions.

We illustrate the dependence of the distortion profile on body permeability by considering the special case of two-dimensional Darcy flow past a permeable cylinder. The flow is described by the velocity potential

$$\phi(r,\theta) = \begin{cases} U\left(1+\dfrac{d}{r^2}\right) r\cos\theta, & r > a, \\ \dfrac{2U\kappa}{(1+\kappa)} r\cos\theta, & r < a, \end{cases}$$

where $d = a^2(1-\kappa)/(1+\kappa)$ is the dipole strength characterizing the far-field flow. Figure 4*a* shows the effect of the cylinder permeability on the flow past an isolated cylinder (streamlines shown in the inset), as well as the associated distortion of a material surface. When $\kappa > 1$, fluid passes preferentially through the cylinder and so the material surface is displaced backwards. When the cylinder has a low permeability ($\kappa \ll 1$), fluid is generally diverted around the cylinder but a finite volume slowly permeates through. Fluid within a distance $2a\kappa$ of the centreline flows through the cylinder where it is retained for a time $O(a/U\kappa)$; consequently, the distorted interface is displaced a large distance $O(a/\kappa)$ forward.

The length-scale L characterizing the deformation of the material surface is shown in figure 4*b*. Here we see that L is singular for cylinders of low permeability because a *finite* volume of fluid permeates through the cylinder with a velocity κU, and is displaced a distance a/κ forward; consequently, $L = O(a/\kappa)$. The corresponding results for the flow around a permeable sphere are also shown. When the permeability of the sphere is low, fluid within a distance $a\sqrt{\kappa}$ of the centreline is displaced a distance $O(a/\kappa)$ forward and consequently $L = O(a/\kappa)$; the singularity of L is a generic feature of flow past bodies of low permeability. When the bodies are highly permeable, L/a tends to a constant value.

4. Mechanical dispersion

We consider potential flow past an assemblage of bodies, and demonstrate that the longitudinal dispersivity may be calculated by tracing the evolution of a material surface advected by the flow. The flow interaction between adjacent bodies in a potential flow is weak because the velocity decays rapidly with distance from the body. Consequently, when the volume concentration is small ($\alpha \ll 1$), the deformation of the material surface is determined correctly to $O(\alpha)$ by superimposing the drift and reflux components associated with individual bodies. In addition, when the material surface has been advected a distance greater than $O(W)$ past a body, the reflux component of displacement $x_r = D_f/A$ is constant across the periodic flow (Eames *et al.* 1994), so that the deformation of the material surface by N bodies is

$$x_f(x_0, y, z, t) = -Ut + \sum_{j=1}^{N} x_d(y - y_j, z - z_j, t) + Nx_r + O(\alpha a), \tag{4.1}$$

where $x_d(y-y_j, z-z_j, t)$ is the drift component of the distortion of a material surface by the single body centred at (x_j, y_j, z_j). For times t such that $(Ut+x_0-x_j)/a \gg 1$, the drift profile assumes a constant form, and for $(Ut + x_0 - x_j)/W > O(1)$, the reflux component is constant across the periodic flow.

The displacement of the material surface in the direction of the flow is x_f, so that the variance of displacement of the distorted material surface is

$$\sigma^2(t) = \frac{1}{A}\int_{\mathcal{A}} (x_f(x_0, y, z, t) - \overline{x_f}(t))^2 \,\mathrm{d}A,$$

where

$$\overline{x_f}(t) = \frac{1}{A}\int_{\mathcal{A}} x_f(x_0, y, z, t) \,\mathrm{d}A \tag{4.2}$$

is the mean position of the surface and, again, A is the cross-sectional area of the periodic domain $\mathcal{A}$. The long-time longitudinal dispersion coefficient, $\mathcal{D}_{xx}$, is defined as half the rate of change of the variance of longitudinal displacement, σ^2 (Batchelor & Townsend 1956):

$$\mathcal{D}_{xx} = \lim_{t\to\infty} \frac{1}{2}\frac{\mathrm{d}\sigma^2(t)}{\mathrm{d}t} = \lim_{t\to\infty} \frac{\sigma^2(t)}{2t}. \tag{4.3}$$

We are thus able to characterize the longitudinal mechanical dispersivity of potential flow past an array of bodies purely in terms of the deformation of a material surface advected by the flow.

We consider the case in which the bodies are fixed and randomly positioned; consequently, the deformation due to each body is statistically independent and the variance of displacement (as $N \to \infty$) is

$$\sigma^2(t) = \frac{1}{A}\left(\sum_{i=1}^{N}(\lim_{t\to\infty} x_{\mathrm{d}}(y-y_i, z-z_i, t) - D_f/A)\right)^2$$
$$\to \frac{1}{A}\sum_{i=1}^{N}(\lim_{t\to\infty} x_{\mathrm{d}}(y-y_i, z-z_i, t) - D_f/A)^2. \tag{4.4}$$

The number of bodies which have passed through the interface is $N = Ut\alpha A/\mathcal{V}$, so that

$$\mathcal{D}_{xx} = \lim_{t\to\infty}\frac{\sigma^2(t)}{2t}$$
$$= \lim_{t\to\infty}\frac{1}{2tA}\sum_{i=1}^{N}\int_{\mathcal{A}}(x_{\mathrm{d}}(y_i, z_i) - D_f/A)^2\,\mathrm{d}A$$
$$= \frac{\alpha U}{2\mathcal{V}}\left(\int_{\mathcal{A}} {x_{\mathrm{d}}}^2\,\mathrm{d}A - \frac{D_f^2}{A}\right). \tag{4.5}$$

The periodic domain is much larger than the body size and, consequently, the second term on the right-hand side of (4.5) is much larger than the first by a factor $|D_f|/AL \ll 1$. Moreover, the integral of x_{d}^2 over the cross-section of the periodic domain, $\mathcal{A}$, may be replaced by the integral over an unbounded region, $\mathcal{A}_\infty$. The longitudinal dispersivity is

$$\mathcal{D}_{xx} = \frac{\alpha U}{2\mathcal{V}}\int_{\mathcal{A}_\infty} {x_{\mathrm{d}}}^2\,\mathrm{d}A. \tag{4.6}$$

An alternative argument, which may be applied to derive (4.6), is provided in the analysis of Acrivos *et al.* (1992), who calculated the longitudinal diffusion of particles in Stokes flow (see their § 2). The time taken for the dispersivity to tend to the limiting value in (4.6) is $UT \gg \max(\mathcal{V}/A\alpha, L)$; consequently, the dispersive process is Fickian for times $t > T$.

The longitudinal mechanical dispersivity associated with the potential flow past an array of bodies may alternatively be expressed as

$$\mathcal{D}_{xx} = \alpha U\frac{|D_f|L}{\mathcal{V}}. \tag{4.7}$$

This general expression for the longitudinal dispersivity in terms of the drift volume, D_f, and L represents the principal contribution of this paper. Using the results of § 3 for the drift volume D_f and length-scale L for flow past individual bodies, it is now straightforward to deduce the explicit form of the coefficient of longitudinal dispersivity, $\mathcal{D}_{xx}$, for a number of special cases, and to interpret the dependence of $\mathcal{D}_{xx}$ on body shape and permeability.

(*a*) *Impermeable bodies*

When the bodies are impermeable ($\kappa = 0$), we have seen in § 3*a* that the drift volume is given by the product of the body volume and the added mass coefficient, $D_f = C_{xx}\mathcal{V}$; consequently, the coefficient of longitudinal dispersivity is simply

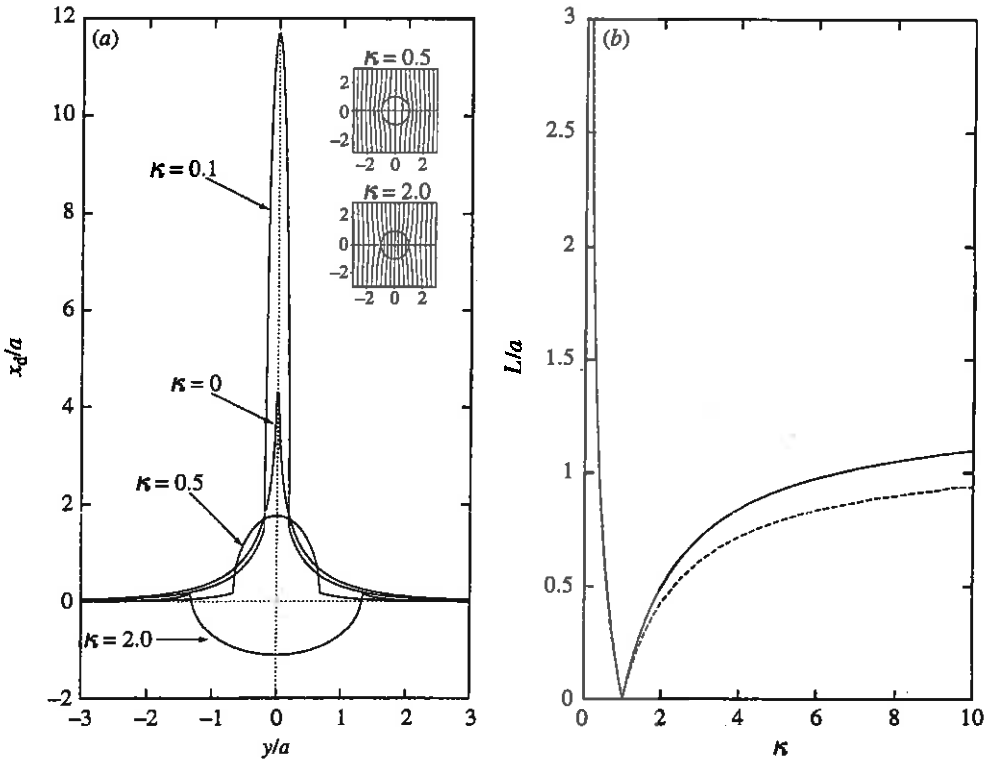

Figure 4. (*a*) The distortion of a material surface by a rigid cylinder ($a/b = 1.0$), of permeability $\kappa = 0$, 0.1, 0.5, 2.0. (*b*) The length-scale, L, characterizing the centre of volume of the D_f, calculated numerically as a function of body permeability, κ, for the case of a cylinder (——) and sphere (– – –).

expressed as $\mathcal{D}_{xx} = \alpha C_{xx} U L$. In this form, we can see that bluff bodies, which are characterized by large values of C_{xx}, enhance mechanical dispersion by increasing the longitudinal stretching of fluid elements.

We return to the special case considered in § 3 *a* of an oblate ellipse aligned with the mean flow, for which $C_{xx} = a/b$. The longitudinal dispersivity associated with an array of ellipses aligned with the mean flow is $\mathcal{D}_{xx} = \alpha U 2\mathcal{C}a^2/(a+b)$. When $a/b \gtrsim 2$ (see figure 2*b*), L is independent of the ellipse length and $\mathcal{D}_{xx} = 2\mathcal{C}\alpha U a^2/b$. Figure 5*a* illustrates the dependence of the coefficient of longitudinal dispersivity on the aspect ratio of the two-dimensional ellipse and three-dimensional ellipsoids aligned with the mean flow, and demonstrates the validity of the scaling results for oblate bodies. For an oblate ellipsoid, when $a/b \gtrsim 5$, $L = 0.81a$ and $C_{xx} \sim 2a/\pi b$, so that the longitudinal dispersivity is $\mathcal{D}_{xx} = 0.52\alpha U a^2/b$.

For ellipses inclined at an angle θ to the mean flow, the longitudinal dispersivity may be calculated analytically (Appendix A) to be

$$\mathcal{D}_{xx} = \alpha U \frac{2\mathcal{C}a^3}{b(b+a)} \left(\frac{a}{b} \cos^2\theta + \frac{b}{a} \sin^2\theta \right)^2.$$

Figure 5*b* shows the variation of $\mathcal{D}_{xx}$ with θ for $a/b = 1, 2, 3, 4$. As θ increases or

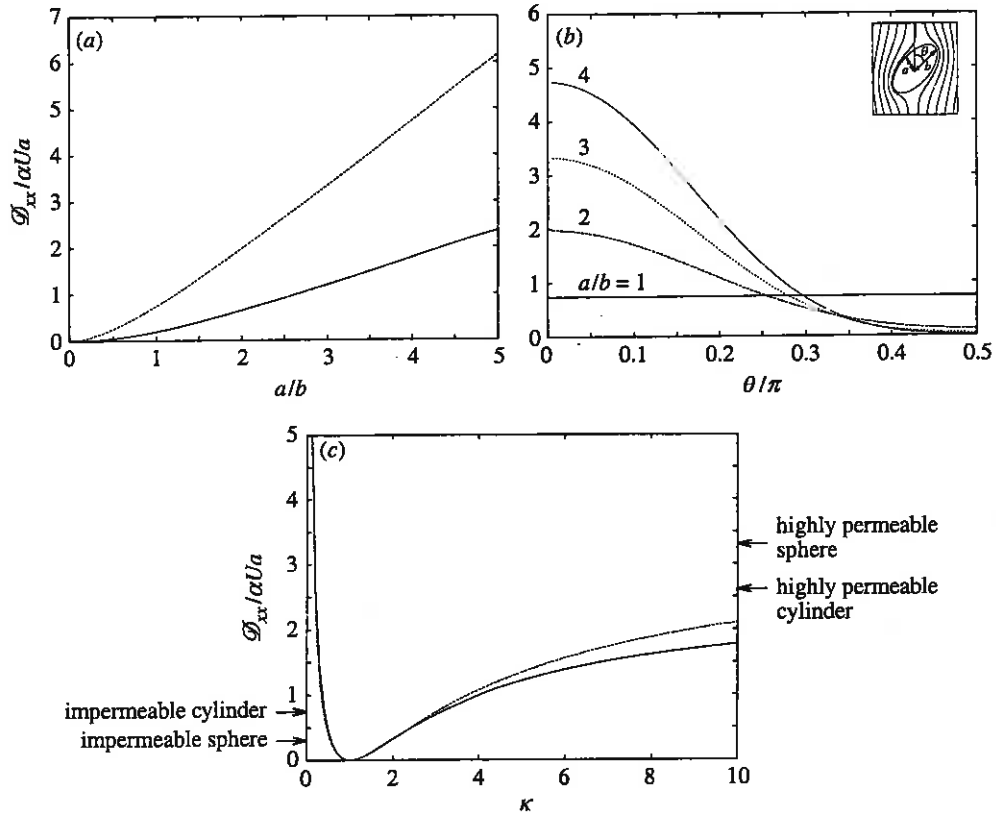

Figure 5. (*a*) The variation of the longitudinal dispersivity, $\mathcal{D}_{xx}$, with aspect ratio for impermeable ellipses (– – –), and ellipsoids (——) aligned parallel to the mean flow. (*b*) The variation of $\mathcal{D}_{xx}$ with the angle of inclination of the ellipse to the mean flow. (*c*) The variation of $\mathcal{D}_{xx}$ with body permeability κ, for porous cylinders (——) and spheres (– – –). The limiting values of the dispersivity for impermeable and highly permeable cylinders and sphere are indicated.

as the aspect ratio of the ellipse decreases, the longitudinal dispersivity decreases significantly (as indicated by figure 5*b*) because the cross-sectional area presented by the ellipse to the mean flow decreases.

(*b*) *Permeable bodies*

When $0 < \kappa \ll 1$, the longitudinal dispersivity is $\mathcal{D}_{xx} = \alpha(C_{xx} + 1)UL$. We have seen in § 3 *b* that the length-scale L is singular for a permeable cylinder as $\kappa \to 0$, owing to the long retention time of a finite volume of fluid within the body. Figure 4*b* shows the variation of the longitudinal dispersivity with permeability for permeable cylinders and spheres, and clearly illustrates the associated singularity in dispersivity as $\kappa \to 0$, which is a generic feature of flow past bodies of low permeability. This singularity was also a feature of the analysis of Magnico *et al.* (1993), who modelled the tracer transport in terms of a one-dimensional random walk, and demonstrated that when $\kappa \ll 1$, the longitudinal dispersivity is $\mathcal{D}_{xx} \sim Ua/\kappa$.

Table 1. *The longitudinal dispersivity, $\mathcal{D}_{xx}$, normalized by $\alpha U a$, for a dilute random array of cylinders and spheres.*

(The asymptotic expressions for $\kappa \to 1$ and $\kappa \to 0$ were calculated using (3.3) and (4.7), and checked against numerical solutions.)

	impermeable	$\kappa \to 0$	$\kappa \to 1$	$\kappa \to \infty$
cylinder	0.74	$\frac{8}{3\pi\kappa}$	$\frac{8}{3\pi}(1-\kappa)^2$	2.59
sphere	0.38	$\frac{1}{3\kappa}$	$\frac{3}{4}(1-\kappa)^2$	3.34

For the case of two-dimensional highly permeable bodies, the longitudinal dispersivity is $\mathcal{D}_{xx} = \alpha(C_{yy}+1)UL$. In this high-$\kappa$ limit, the longitudinal dispersivity is *enhanced* by slender bodies, which are characterized by large values of C_{yy}, and the influence of body shape on longitudinal dispersivity is seen to be opposite in the high- and low-κ limits. The limiting values of $\mathcal{D}_{xx}$ as $\kappa \to \infty$ are indicated in figure 4*b* and table 1, and show that highly permeable spheres generate greater longitudinal dispersion than highly permeable cylinders, which is contrary to when they are impermeable. The examples chosen are point-symmetric bodies, which do not illustrate the strong tendency of the flow to be focused by highly permeable slender bodies, an effect discussed by Phillips (1991).

5. Mixing across a horizontal interface

We proceed by applying our simple model of mechanical dispersion in order to examine the efficiency of the bodies in mixing across a horizontal interface. Consider two superposed fluids, the upper being clear and the lower dyed, initially separated by a horizontal interface $x = 0$. The horizontally averaged dye concentration is given initially by $\overline{C} = 0$ $(x > 0)$ and $\overline{C} = 1$ $(x < 0)$. At some time $t = 0$, bodies begin to pass through the interface, thus distorting it and smoothing out the step in $\overline{C}(x)$ through mechanical dispersion. This is essentially the method used to determine experimentally the longitudinal dispersivity associated with the flow through a porous sample, where the initial step change in concentration corresponds to the injection of a salt or dye. The longitudinal dispersivity is measured from the horizontally average concentration profile at the exit of the sample of porous media. Magnico *et al.* (1993) used this method in their experimental study of dispersion by beads of low permeability, and observed that when the mean transit time of the tracer through the sample was comparable to the residence time within the beads (i.e. $Ut \sim L$), the concentration profile was non-Gaussian. In this discussion of the evolution of $\overline{C}$, we restrict our analysis to the limit of $Ut \gg \max(L, \mathcal{V}/\alpha A)$, for which the longitudinal dispersivity is constant and $\overline{C}$ spreads as a Gaussian profile.

We have shown that the dispersive process is Fickian for large time so that the horizontally averaged concentration field $\overline{C}$ satisfies

$$\frac{\partial \overline{C}}{\partial t} + \frac{\mathrm{d}\overline{x}_f(t)}{\mathrm{d}t}\frac{\partial \overline{C}}{\partial x} = \mathcal{D}_{xx}\frac{\partial^2 \overline{C}}{\partial x^2}. \tag{5.1}$$

The mean displacement of the material surface calculated from (3.6) and (3.9) is $\overline{x}_f(t) = -\epsilon \mathcal{V} N/A$, where N is the number of bodies which have passed through the

surface. The mean velocity of the material surface relative to the bodies is

$$\frac{\mathrm{d}\overline{x_f}(t)}{\mathrm{d}t} = \frac{\overline{x_f}(t)}{t} = -U(1+\epsilon\alpha), \tag{5.2}$$

which is increased relative to the free stream speed $-U$ by the retention of fluid by the bodies. Substituting (4.7) and (5.2) into (5.1) gives

$$\frac{\partial \overline{C}}{\partial t} - U(1+\epsilon\alpha)\frac{\partial \overline{C}}{\partial x} = \alpha U \frac{|D_f|L}{\mathcal{V}}\frac{\partial^2 \overline{C}}{\partial x^2}. \tag{5.3}$$

The horizontally averaged concentration field $\overline{C}$ changes owing to reflux, which shifts the interface at a speed $U(1+\epsilon\alpha)$, and to the mechanical dispersion associated with the body-scale distortions of the interface.

We examined the variation of the concentration field with time by considering the deformation of a material surface by a number of bodies. Figure 6*a–c* shows the deformation of a material surface by a number of high permeability cylinders ($\kappa = 2$) which have risen through the interface. As N increases, the deformation of the interface becomes more pronounced. Figure 6*d* shows the evolution of the horizontally averaged dye concentration profiles with increasing N. Initially the concentration profiles are heavily skewed; however, the skewness decreases as N increases. For the sake of comparison, the Gaussian profile, anticipated on the basis of (5.3), is shown.

6. Diffusive effects at high Péclet number

The results for mechanical dispersivity have been calculated by neglecting the effects of tracer diffusivity. We proceed by considering the influence of weak diffusive effects and so examine the limit of large, but not infinite, Pe. The impact of diffusion on dispersion is important in regions, such as near stagnation points or within low permeability bodies, where the flow is slowly moving relative to the stream velocity U. When $\kappa > 0$, there are no stagnation points in the flow and the minimum flow speed is typically $U\min(1, O(\kappa))$, so that diffusive effects can be ignored everywhere when the Péclet number defined in terms of the minimum local flow speed is large, i.e. $Pe \gg \max(1, 1/\kappa)$. When the bodies are characterized by a low permeability, such that κPe is small, diffusion is important within the bodies. Although the diffusive component of tracer transport is not treated in this paper, the appropriate scaling for $\mathcal{D}_{xx}$ may be anticipated by considering tracer particles which remain trapped within the bodies for a time $a^2/\mathcal{D}_1$, where $\mathcal{D}_1$ is the molecular diffusivity within the bodies, before leaving by cross-streamline diffusion. Tracer hold-up makes a contribution of order $\alpha U^2 a^2/\mathcal{D}_1$ to the longitudinal dispersivity. Hence, in the $\kappa Pe \ll 1$ regime, the longitudinal dispersion is dominated by diffusive effects and $\mathcal{D}_{xx} = O(\alpha U^2 a^2/\mathcal{D}_1)$. A similar contribution to dispersivity was found by Koch & Brady (1985) from tracer hold-up within rigid spheres fixed in a Stokes flow.

For flow past impermeable bodies, diffusive effects are only important at the stagnation points on the body surface. Since these stagnation regions are small and localized, they make a negligible contribution to the longitudinal dispersion. We thus conclude that the coefficient of longitudinal dispersion is $\mathcal{D}_{xx} = \alpha C_{xx} UL + \mathcal{D}_2$, for potential flows past impermeable bodies for $Pe \gg 1$.

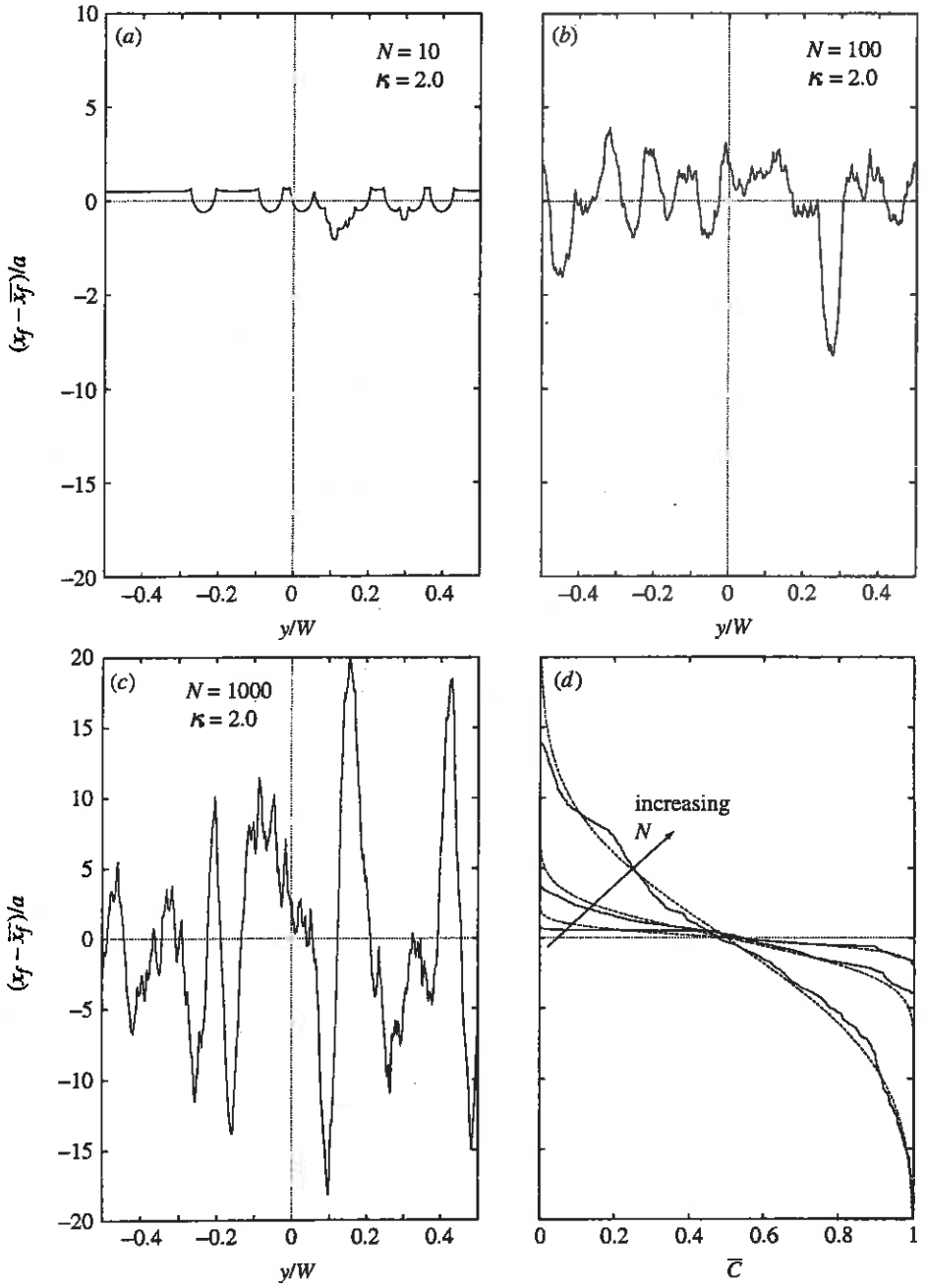

Figure 6. The time evolution of an initially horizontal material surface distorted by permeable cylinders ($\kappa = 2$) rising though a periodic channel ($W/a = 40$): (*a*) $N = 10$, (*b*) $N = 100$, (*c*) $N = 1000$. The associated evolution of the horizontally averaged concentration field is shown in (*d*) as (——), along with the profiles predicted theoretically by (5.3) (– – –).

Table 2. *The longitudinal dispersivity arising from the potential flow past two- or three-dimensional impermeable bodies, at large and small Péclet number* $Pe(= Ua/\mathcal{D}_2)$.

(The low-Péclet-number results are derived by applying Maxwell's (1873) method of calculating $\mathcal{D}_{xx}$ for cylinders and spheres to arbitrary shaped bodies. The table demonstrates that bluff bodies enhance $\mathcal{D}_{xx}$ at high Pe by increasing the stretching of fluid elements, whereas bluff bodies reduce $\mathcal{D}_{xx}$ in the limit of low Pe.)

flow regime	longitudinal dispersivity $\mathcal{D}_{xx}$
$Pe \ll 1$	$(1-\alpha(1+C_{xx}))\mathcal{D}_2$
$Pe \gg 1$	$\alpha U C_{xx} L$

7. Concluding remarks

We have examined the effect of body shape and permeability on dispersion by bodies randomly positioned in a potential flow. We have quantified the longitudinal dispersivity in the high Péclet limit, and shown that diffusive effects are negligible for impermeable bodies at high Pe and for permeable bodies provided $Pe \gg \max(1, 1/\kappa)$. In these cases, the longitudinal dispersivity may be calculated by examining the deformation of a material surface advected through an array of bodies. We have expressed the coefficient of longitudinal dispersivity as $\mathcal{D}_{xx} = \alpha U|D_f|L/\mathcal{V}$, and found that the influence of body permeability on the longitudinal dispersion is quite dramatic (see table 1). When the bodies are impermeable (table 2), the dispersivity is increased by body bluffness, which serves to enhance the longitudinal stretching of fluid elements. The longitudinal dispersivity increases significantly as $\kappa \to 0$ owing to the long-time retention of fluid within the bodies. In the high-κ limit, fluid passes preferentially through the bodies, and slender rather than bluff bodies enhance longitudinal dispersion.

We have shown that the longitudinal dispersivity increases significantly in the limit of vanishingly small permeability, providing that diffusive effects are negligible, $Pe \gg \max(1, 1/\kappa)$. The enhancement of dispersivity at low κ does not reflect the breakdown of the mathematical model, and its physical significance is underlined by the experimental study by Magnico *et al.* (1993), who showed that the longitudinal dispersivity associated with the flow past a fixed array of porous spherical beads increased significantly (by a factor of about five) as the relative permeability of the beads decreased (by a factor of about 10). Magnico *et al.* (1993) argued, as we have, that when $\kappa Pe \gg 1$, diffusive effects may be ignored within the beads and the longitudinal dispersivity is dominated by the flow through the beads and the dispersivity is $\mathcal{D}_{xx} \sim Ua/\kappa$. This singularity in dispersivity also has a bearing on numerical simulations of dispersion in ground water. For instance, Wheatcraft *et al.* (1990) studied dispersion through a fractal porous material consisting of impermeable inclusions, using a value of $\kappa = 0.01$ in order to avoid computational problems experienced when $\kappa = 0$. The results of this paper suggest that additional care must be taken when bodies of low permeability are embedded in the flow and that their impact on the flow may be significant, even when their volume fraction is low, i.e. even when α is $O(\kappa)$. We should note that as $\kappa \to 0$, diffusive effects become increasingly important within the regions of low permeability and provide an upper bound for the longitudinal dispersivity of $O(\alpha a^2 U^2/\mathcal{D}_1)$.

Bubble-induced mixing is used in a variety of industrial processes, and is in general influenced by both the transport properties of individual bubbles, and those associated with the large-scale convective overturnings established by gradients in bubble concentration. The flow upstream of a high-Reynolds-number bubble may be described to leading order by potential flow theory; however, the inviscid flow description breaks down in a thin boundary layer adjoining the bubble and in the trailing wake (Moore 1965). The fluid transport associated with the rise of individual high-Reynolds-number bubbles was studied by Bhaga & Weber (1981) and more recently by Bush & Eames (1998), who demonstrated that the contribution made by the inviscid flow component to fluid transport was significant. While the flow generated by rising bubbles is unsteady and the position of the bubbles is not fixed relative to one another, we may still gain some insight into bubble-induced mixing by applying our potential flow model. Our results indicate the dependence of dispersivity on the aspect ratio a/b of oblate ellipsoids, $\mathcal{D}_{xx} = 0.26\alpha U d_e (a/b)^{4/3}$, where the effective diameter of an ellipsoid is $d_e = 2(a^2 b)^{1/3}$. Consequently, we anticipate that the dispersive properties of high-Reynolds-number bubbles rising in water, whose aspect ratio (Clift *et al.* 1978) varies from $a/b = 1$–5 as the Reynolds number increases from 100 to 1500, are extremely sensitive to the Reynolds number. There may be other important contributions to the mixing processes from the trailing vorticity or unsteady bubble motion; consequently the potential flow description presented here yields a lower bound for the longitudinal dispersivity.

The results we have derived for a random array of identical bodies may be extended to the general case where the body geometry and permeability are variable. By following the arguments used to derive (4.7), we can demonstrate that the longitudinal dispersivity associated with a random array of bodies is

$$\mathcal{D}_{xx} = \int \frac{\alpha_\beta U |D_f|_\beta L_\beta}{\mathcal{V}_\beta} \, \mathrm{d}\beta, \quad Pe \gg 1, \tag{7.1}$$

where α_β is the volume fraction of bodies with a prescribed geometry and permeability specified by the dummy variable β. These results provide some insight into dispersion arising from a random permeability distribution. For instance, Dagan (1984) showed that when the random permeability field is spatially correlated over a distance I, the longitudinal dispersivity is $\mathcal{D}_{xx} = UI\sigma_Y^2$. This result could be anticipated from table 1 (as $\kappa \to 1$), because the regions with relative permeability $1 \pm O(\sigma_Y)$ dominate longitudinal dispersion and have a characteristic length I, so that $\mathcal{D}_{xx} = O(UI\sigma_Y^2)$. When the permeability field of an assemblage of identical bodies is characterized by a lognormal distribution, the longitudinal dispersivity may be calculated from (7.1). The longitudinal dispersivity associated with arrays of permeable cylinders and spheres may be calculated using (7.1) and table 1 and are, respectively (Appendix B),

$$\mathcal{D}_{xx} = \frac{8}{3\pi}\alpha U a \sigma_Y^2 \quad \text{and} \quad \mathcal{D}_{xx} = \tfrac{3}{4}\alpha U a \sigma_Y^2.$$

Finally, the results in this paper have motivated an experimental study of dispersion by potential flow, which may be achieved using a Hele–Shaw cell (Bear 1972), and which is currently being undertaken by the authors.

I.E. acknowledges the support through the Jeremy Howarth Fellowship at St Catharine's College. J.W.M.B. acknowledges support from NERC Bridge grant GST/02/1147. The authors thank Dr

Victoria Saporta for helpful suggestions and Dr John Hinch for a number of valuable discussions and comments on the paper.

Appendix A.

We demonstrate that the deformation of a material surface by an ellipse inclined in a uniform stream corresponds to that caused by a cylinder of radius $\frac{1}{2}(a+b)$. This result may be established using the complex variable formulation of the potential flow problem. The flow around an ellipse may be mapped from the z-plane to the ζ-plane to the flow around a cylinder of radius $c = \frac{1}{2}(a+b)$ (see Batchelor 1967, p. 428). The transformation $z(\zeta) = \zeta + \lambda^2/\zeta$, where $\lambda^2 = \frac{1}{4}(a^2 - b^2)$, maps the ellipse to a cylinder in the ζ-plane. The flow in the ζ-plane corresponding to the flow past a cylinder gives $w(\zeta) = U(\zeta - c^2 \mathrm{e}^{-2\theta \mathrm{i}}/\zeta)$. The fluid displacement due to the flow past the ellipse is

$$x_{\mathrm{d}}(\psi) = \int_{-\infty}^{\infty} \frac{q^2}{U}\,\mathrm{d}t = \int_{-\infty}^{\infty} \left[\left(\frac{\mathrm{d}w}{\mathrm{d}z} - 1\right)\overline{\left(\frac{\mathrm{d}w}{\mathrm{d}z} - 1\right)} \Big/ \left(\frac{\mathrm{d}w}{\mathrm{d}z}\overline{\frac{\mathrm{d}w}{\mathrm{d}z}}\right)\right] \frac{\mathrm{d}\phi}{U},$$

where the overbar denotes the complex conjugate. Transforming the integrand to the $\zeta-$plane,

$$x_{\mathrm{d}}(\psi) = \int_{-\infty}^{\infty} \left(\frac{\mathrm{d}w}{\mathrm{d}\zeta} - \frac{\mathrm{d}z}{\mathrm{d}\zeta}\right)\overline{\left(\frac{\mathrm{d}w}{\mathrm{d}\zeta} - \frac{\mathrm{d}z}{\mathrm{d}\zeta}\right)} \frac{\mathrm{d}t'}{U}, \tag{A 1}$$

where the time t' is defined by

$$\frac{\mathrm{d}\phi}{t'} = \frac{\mathrm{d}w}{\mathrm{d}\zeta}\overline{\frac{\mathrm{d}w}{\mathrm{d}\zeta}}.$$

Substituting for $w(\zeta)$ and $z(\zeta)$ into (A 1) shows that

$$x_{\mathrm{d}}(\psi) = \frac{2ab}{a+b}\left(\frac{a}{b}\cos^2\theta + \frac{b}{a}\sin^2\theta\right)\left(\int_{-\infty}^{\infty} \frac{c^3}{|\zeta|^4}\frac{\mathrm{d}t'}{U}\right). \tag{A 2}$$

The integral on the right-hand side corresponds to the fluid displacement by a cylinder of radius c, normalized by the length-scale c. The length-scale L defined by (3.5) for an ellipse aligned with the flow may be calculated from (A 2) to be

$$\frac{L}{a} = \frac{2Cb}{a+b}\left(\frac{a}{b}\cos^2\theta + \frac{b}{a}\sin^2\theta\right),$$

where $C = 0.74$. The longitudinal dispersivity due to a dilute random array of ellipses is thus

$$\mathcal{D}_{xx} = \alpha U \frac{2Cb}{a+b}\left(\frac{a}{b}\cos^2\theta + \frac{b}{a}\sin^2\theta\right).$$

Appendix B.

When $\sigma_Y \ll 1$, the longitudinal dispersivity, $\mathcal{D}_{xx}$, associated with an assemblage of cylinders whose permeability is characterized by a lognormal distribution, may be

calculated from (7.1) and table 2:

$$\begin{aligned}\mathcal{D}_{xx} &= \frac{8}{3\pi}\alpha U a \int_{-\infty}^{\infty}(1-\kappa)^2 \frac{1}{\sqrt{2\pi}\sigma_Y \kappa}\exp\left(-\frac{(\log\kappa)^2}{2\sigma_Y^2}\right)\mathrm{d}\kappa \\ &= \frac{8}{3\pi}\alpha U a(1-2\exp(\tfrac{1}{2}\sigma_Y^2)+\exp(2\sigma_Y^2)) \\ &= \frac{8}{3\pi}\sigma_Y^2\alpha U a + O(\alpha U a \sigma_Y^4).\end{aligned}$$

The corresponding result for an array of spheres may be calculated by the same method.

References

Acrivos, A., Batchelor, G. K., Hinch, E. J., Koch, D. L. & Mauri, R. 1992 Longitudinal shear-induced diffusion of spheres in a dilute suspension. *J. Fluid Mech.* **240**, 651-657.

Batchelor, G. K. 1967 *An introduction to fluid dynamics.* Cambridge University Press.

Batchelor, G. K. & Townsend, A. A. 1956 Turbulent diffusion. In *Surveys in mechanics*, pp. 352–399. Cambridge University Press.

Bear, J. 1972 *Dynamics of fluids in porous media.* New York: Dover.

Bhaga, D. & Weber, M. E. 1981 Bubbles in viscous liquids: shapes, wakes and velocities. *J. Fluid Mech.* **105**, 61–85.

Bush, J. W. M. & Eames, I. 1998 Fluid displacement by high *Re* number bubbles in a thin gap. *Int. Jl Multiphase Flow* **24**, 411–430.

Chang, C. C. 1992 Potential flow and forces for incompressible viscous flow. *Proc. R. Soc. Lond.* A **437**, 517–525.

Clift, R., Grace, J. R. & Weber, M. E. 1978 *Bubbles, drops and particles.* New York: Academic.

Dagan, G. 1984 Solute transport in hetergeneous porous formations. *J. Fluid Mech.* **145**, 151–177.

Dagan, G. 1987 Theory of solute transport by groundwater. *A. Rev. Fluid Mech.* **19**, 183–215.

Drazin, P. G. 1961 On the steady flow of fluid of variable density past on obstacle. *Tellus* **13**, 239–251.

Darwin, C. 1953 A Note on hydrodynamics *Proc. Camb. Phil. Soc.* **49**, 342–354.

Eames, I., Belcher, S. E. & Hunt, J. C. R. 1994 Drift, partial drift and Darwin's proposition. *J. Fluid Mech.* **275**, 201–223.

Freeze, R. A. 1975 A stochastic-conceptual analysis of one-dimensional groundwater flow in nonuniform homogeneous media. *Water Resources Res.* **11**, 725–741.

Havelock, T. 1911 The displacement of the particles in the case of fluid motion. *Proc. Durham Phil. Soc.* **IV**, 81-91.

Hunt, J. C. R. 1973 A theory of turbulent flow around two-dimensional bluff bodies. *J. Fluid Mech.* **61**, 625–706.

Hunt, J. C. R. & Mulhearn, P. J. 1973 Turbulent dispersion from sources near two-dimensional obstacles. *J. Fluid Mech.* **61**, 245–274.

Jerram, N., Perkins, R. J., Fung, J. C. H., Davidson, M. J., Belcher, S. E. & Hunt, J. C. R. 1995 Atmospheric flow through groups of buildings and dispersion from localised sources. In *Wind climate in cities* (ed. J. E. Cerrank, A. G. Davenport, E. J. Plate & D. X. Viegas), pp. 109–130. Dordrecht: Kluwer.

Koch, D. L. & Brady, J. F. 1985 Dispersion in fixed beds. *J. Fluid Mech.* **154**, 399–427.

Magnico, P., Leroy, C., Brouchaud, J. P., Gaulthier, C. & Hulin, J. P. 1993 Tracer dispersion in porous media with double porosity. *Phys. Fluids* **5**, 46–57.

Maxwell, J. C. 1870 On the displacement in a case of fluid motion. *Proc. Lond. Math. Soc.* **3**, 82–97.

Moore, D. 1965 The velocity of rise of a distorted gas bubble in a liquid of small viscosity. *J. Fluid Mech.* **23**, 749–765.

Phillips, O. M. 1991 *Flow and reaction in permeable rocks.* Cambridge University Press.

Pozrikidis, C. 1996 *Introduction to theoretical and computational fluid dynamics.* Oxford University Press.

Rankine, W. J. M. 1864 On plane water-lines in two dimensions. *Phil. Trans. R. Soc. Lond.* A **154**, 369–391.

Rowe, P. N. 1962 The effect of bubbles in gas–solid contacting in fluidized beds. *Chem. Engng Prog. Symp.* **58**, 42–56.

Saffman, P. G. 1959 A theory of dispersion in a porous medium. *J. Fluid Mech.* **6**, 321–349.

Taylor, G. I. 1928 The energy of a body moving in an infinite fluid, with an application to airships. *Proc. R. Soc. Lond.* A **120**, 13–21.

Weng, W. S. & Carruthers, D. J. 1994 Modelling turbulent diffusion from a point source in strongly stratified flow around a three-dimensional arbitrarily shaped hill. In *IMA stably stratified flows: flow and dispersion over topography* (ed. I. P. Castro & N. J. Rockliff), pp. 263–274. Oxford University Press.

Wheatcraft, S. W., Sharp, G. A. & Tyler, S. W. 1990 Fluid flow and transport in fractal heterogeneous porous media. In *Dynamics of fluids in hierarchical porous media* (ed. J. H. Cushman), pp. 305–326. New York: Academic.

Yih, C.-S. 1985 New derivations of Darwin's theorem. *J. Fluid Mech.* **152**, 163–172.